Chapter 1

Introduction

About a century ago, the knowledge of the universe was little more advanced than that in the Stone Age. But within this last century, our knowledge of the universe evolved at an exponential rate. This has been possible due to the development of various techniques and the advent of telescopes in all different wavebands of the electromagnetic spectrum. When we observe along a different line of sight of the universe, we find that the universe contains a large number of galaxies, each with billions of stars. Observation of Milton L. Humason, Slipher and Hubble eluted that the universe is expanding (Slipher, 1913) but from the first supernovae observation, we came to know that it is also accelerating (Peebles and Ratra, 2003; Perlmutter et al., 1999; Riess et al., 1998). The first theoretical understanding appeared with the General Theory of relativity (GTR) (Einstein, 1915). After combining GTR proposed and Hubble's law, Friedmann (1924), Lemaître (1931), Howard P. Robertson and Arthur Geoffrey Walker came up with the idea of the expanding universe and proposed the model of the universe, which would eventually be called the Big bang Model.

Understanding this subject can shed light on the past, present, and future of the evolving universe. As per today's understanding, the universe is 13.8 billion years old. Its lifetime is divided into various epochs. Present understanding of the universe is based on the

Cosmological Principle which considers that the universe is statistically homogeneous and isotropic at large enough scales. In this work, we will try to probe an epoch of the universe generally known for star formation, galaxy combination and evolution i.e. Post-reionization epoch with neutral hydrogen as a probe with an application of the gravitational lensing technique.

1.1 A very brief history of the Universe

Every object in this universe is moving away from another object with a certain velocity called recessional velocity and this velocity v is directly proportional to the distance between the objects D, $v = H_0 D$ where H_0 is the Hubble's constant and D is the proper distance. Like in the case of the Doppler effect, there is a shift in frequency when there is a relative motion between source and listener. Similarly, there is a shift in frequency or wavelength due to the cosmological expansion of the universe that we generally measure in terms of redshift z and can be written as

$$z = \frac{\lambda_0}{\lambda_e} - 1 \approx \frac{v}{c} \tag{1.1}$$

where λ_0 is the observed wavelength and λ_e is the emitted wavelength of the radiation emitted (Sartori, 1996).

At a very early age, the universe was filled with hot plasma which was opaque to the incident radiation. With time the universe expanded and cooled down. Eventually, when the temperature becomes 3000 K at a redshift of $z \sim 1000$, recombination of proton and electron occurred. This freed the photons from much scattering and resulted in the emission of microwave radiation which is nowadays called cosmic microwave background (CMB) and this epoch is known as the recombination epoch of the universe. This has been thoroughly studied with various experiments like COBE, WMAP and now by Planck

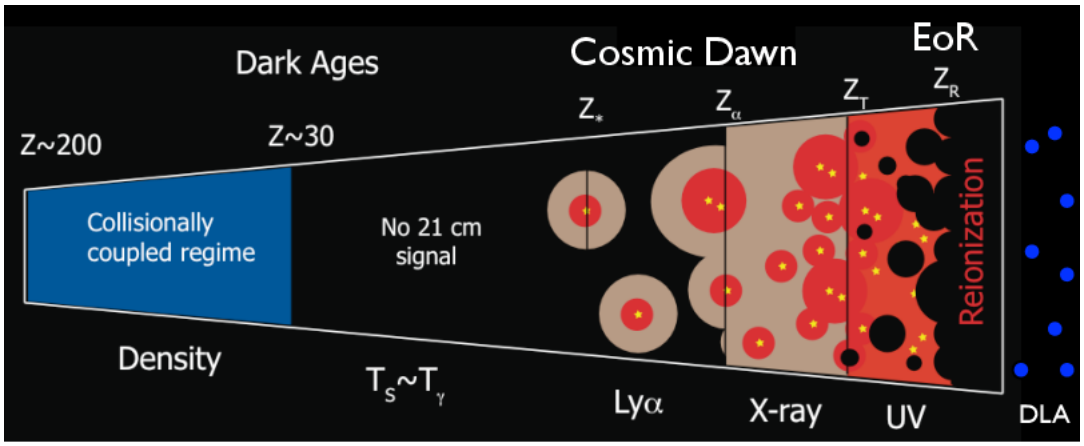

Figure 1.1: Cartoon of the different phases of the Global 21 cm signal. After reionization is complete there is a residual signal from neutral hydrogen in galaxies. Credit: (Pritchard and Loeb, 2012)

satellites (Jarosik et al., 2003; Melchiorri et al., 1981; Planck Collaboration et al., 2020). The CMB map observed from these studies gives information about the initial anisotropies of the universe. As time passed, the universe continued to cool down and expand and the initial density perturbation grew under gravitational instability. Just after the recombination and decoupling of radiation from the matter, the Universe was completely transparent to radiation with no luminous source around. This epoch is known as the Dark Ages (Barkana and Loeb, 2001). Then around at redshift of $z \sim 15$ overdensities collapsed, and there was the formation of the first luminous sources which started to ionize the neutral hydrogen around it (Pritchard and Loeb, 2008). As time passed more and more luminous sources were formed and they ionized the neutral hydrogen around them. This epoch is known as the epoch of reionization. This reionization occurred up to a redshift of $z \sim 6$ (Fan et al., 2006) leaving only a certain region inside the universe which remained shielded and neutral from these radiations. Those regions are called damped Lyman alpha clouds and galaxies. (Doré et al., 2007; Furlanetto et al., 2006; McQuinn, 2016; Zaroubi, 2013). Some of the Lyman alpha studies indicate reionization was more gradual and continued beyond $z \sim 6$ (Kulkarni et al., 2019; Mitra et al., 2015; Weinberger et al., 2020).

There are many different ways to observe this epoch of reionization. The first probe is the CMB radiation, CMB radiation not only possesses the imprints of initial anisotropies of the universe but also of this epoch. Since CMB photons scattered off from free electrons by Thomson scattering induce the secondary anisotropies in the CMB and induce the damping in the primary anisotropies. Polarization dependence of the Thomson cross-section modifies the polarization of the initially anisotropic photon field (Haiman and Knox, 1999). The other source of information of this era is quasar spectra i.e. Gunn Peterson trough, in which we observe a large number of absorption lines in the quasar spectra that predict that the universe is highly ionized at a redshift of $z \sim 5.5$ (Becker et al., 2001). An alternate but extremely promising probe is a redshifted 21 cm emission signal from neutral hydrogen. This is also the most useful technique for studying the different epochs of the universe. We shall focus on the 21 cm signal as a probe of the universe shortly.

At the redshift range $0 \leq z \leq 6$, the major structural change in the universe happens through the formation of galaxies, their mergers and evolution (Mo et al., 2010). The epoch in which this structure formation occurs is known as the post-reionization epoch of the universe. In this epoch H I is mostly trapped in the galaxies, like Damped Lyman-α absorbers, where they are shielded from the ionizing radiation (Furlanetto et al., 2006; Gunn and Peterson, 1965; Lanzetta, 2000; Pritchard and Loeb, 2012). However, there is a significant amount of neutral hydrogen left in the Circumgalactic Medium (CGM) and the Intergalactic Medium (IGM) (McQuinn, 2016). This gas, as time evolves, falls into the galaxies and keeps the star formation engine running (Baugh et al., 1998; Bera et al., 2019; Chowdhury et al., 2020; Kauffmann et al., 1993). Star formation and its feedback also play an important role in the evolution of the large scale H I density (Bothwell et al., 2009; Zhou et al., 2018). It is very difficult to observe the neutral hydrogen distribution inside the galaxies, above the source at redshift $z \sim 0.3$ requires a large observation time (Kanekar

et al., 2016), but one can observe an average neutral hydrogen distribution by using the stacking of a large number of galaxies (Bera et al., 2019; Chowdhury et al., 2020), still, much to be explored to understand its distribution through an observational probe (Arora and Dutta, 2020; Bagla et al., 2010).

1.1.1 21 cm signal emission from Neutral Hydrogen

21 cm signal is emitted due to the spin-flip transition in the ground state of the hydrogen atom. The frequency of the radiation emitted is equal to 1420 MHz and the wavelength is 21 cm (Griffiths, 1982; Hellwig et al., 1970) and was first observed by Ewen and Purcell in 1951 (Ewen and Purcell, 1951). This signal is a key probe to understanding the various eras of the universe. This transition is highly forbidden with an extremely small transition rate of $2.85 \times 10^{-15} sec^{-1}$ that gives a mean lifetime of the excited state of around 10 million years.

We write the excitation temperature for neutral hydrogen for this spin-flip transition as spin temperature T_S which quantifies the ratio of the number densities of atoms in the two hyperfine levels of the electronic ground state.

$$T_S = \frac{\Delta E}{k_B} / \ln \frac{n_0 g_1}{n_1 g_0} \tag{1.2}$$

Here subscript 1 and 0 represents the spin 1 and 0 state, g_i are the statistical weights of the two states (here $g_0 = 1$ and $g_1 = 3$) and $\Delta E = 5.9 \times 10^{-6}$ eV is the energy separation between two states and k_B is the Boltzmann constant.

Another quantity of interest is specific intensity of 21 cm emission from a cloud, We will use Brightness temperature T_b here in place of specific intensity. Using the

Rayleigh-Jeans approximation, the brightness temperature is defined as

$$T_b(\nu) = \frac{I_\nu c^2}{2k_B \nu^2} \tag{1.3}$$

where c is the speed of light, I_ν is the specific intensity and ν the observed frequency. The equation of radiative transfer along a line of sight direction through a cloud of uniform excitation temperature T_S in terms of frequency is

$$T_b(\nu) = T_S(1 - e^{-\tau}) + T_R(\nu)e^{-\tau} \tag{1.4}$$

where T_R is the radiation temperature and τ (Bharadwaj and Ali, 2005; Furlanetto et al., 2006) is the optical depth which involves the effect of stimulated emission, expansion of the universe, Doppler effect i.e. effect of peculiar velocity and neutral hydrogen density fraction as

$$\tau = \frac{4.0mK}{T_S}\left(\frac{\Omega_b h^2}{0.02}\right)\left(\frac{0.7}{h}\right)\frac{H_0}{H(z)}(1+z)^3\frac{\rho_{HI}}{\bar{\rho}_H}\left[1 - \frac{(1+z)}{H(z)}\frac{\partial v}{\partial r_\nu}\right] \tag{1.5}$$

, where r_ν is the comoving distance of the cloud, $\rho_{HI}/\bar{\rho}_H$ is the neutral hydrogen density fraction, $H_0/H(z)$ is the effect of Hubble expansion, term in the square bracket is the effect of peculiar velocity and all other parameters are from Standard ΛCDM cosmology.

Taking the radiation temperature in brightness temperature as the CMB temperature, such that $T_R = T_{CMB}$, the variation of brightness temperature, the CMB temperature for small optical depth, can be written as

$$\delta T_b = \frac{T_S - T_{CMB}}{1+z}\tau \tag{1.6}$$

When $T_S > T_{CMB}$ it corresponds to an emission signal and otherwise corresponds to an absorption signal. The evolution of the spin temperature with redshift is shown in the Fig 1.2

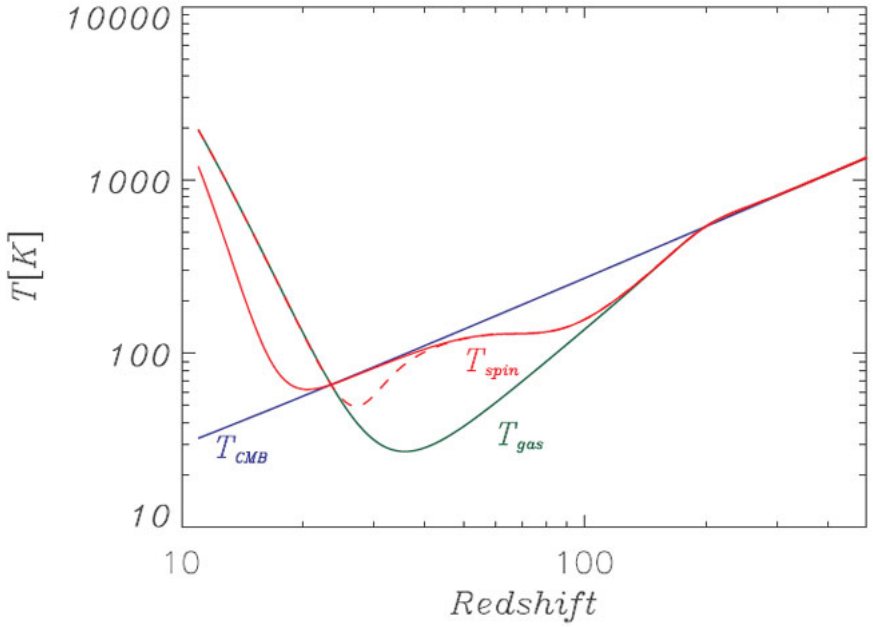

Figure 1.2: The global evolution of the CMB (blue line), gas (green line) and spin (red solid line and red dashed line) temperatures as a function of redshift. The CMB temperature evolves steadily as $1+z$ whereas the gas and spin temperatures evolve in a more complicated manner (see text in detail). (Zaroubi, 2013)

Fig 1.2 shows the expected global evolution of the spin temperature as a function of redshift. The blue solid line represents T_{CMB}, which drops as $1+z$. The green line shows the gas temperature as a function of redshift. At $z \approx 200$, the gas temperature is still coupled to the CMB due to the Compton scattering of the background photons off residual electrons leftover from the recombination era. So $T_b = 0$. Hence there will not be any signal. At $z \sim 200$, however, the gas decouples from the CMB radiation and starts adiabatically cooling as a function of the redshift squared, $(1+z)^2$ and spin temperature is still in coupling with the gas temperature due to collisional coupling resulting in an absorption signal. At $z \approx 100$ the efficiency of collisional coupling to the gas drops due to the Hubble expansion. At $40 \leq z \leq 30$, expansion of the universe continues, reducing the

gas density and radiative coupling causes $T_S \approx T_{CMB}$ resulting in no signal. Two possible histories can exist, one in which T_S couples to the gas as it heats up once it obtains a temperature greater than T_{CMB} (red solid line). In the other possible evolution, the spin temperature couples to the gas much before the kinetic temperature exceeds that of the CMB (red dashed line). In the former case the 21 cm radiation, after decoupling from the CMB at $z \approx 30$, is seen only in emission, whereas in the latter case it is seen initially in absorption and only at later stages in emission. One can see the former case in Fig 1.3 in which we observe an emission signal after $z \approx 30$.

1.1.2 Detection of neutral hydrogen at high redshift

Neutral hydrogen itself is also one of the most promising observational probes in the first billion years of the Universe. 21 cm absorption studies provide an interesting probe of physical conditions in the neutral atomic gas phase in galaxies and other cluster groups (Allison et al., 2022; Glowacki et al., 2017; Kanekar, 2014; Vermeulen et al., 2003). Sunyaev and Zeldovich (1975, 1972) suggested using the redshifted 21 cm hyperfine structure transition of H I to study the distribution of baryonic matter in the post reionization era. One can observe the neutral hydrogen distribution at the various redshifts along the line of sight directions using the quasar absorption spectra. From the semi-analytical or numerical simulation of the self-shielding clouds, Viegas (1995) has found the threshold value of column density for hydrogen cloud is that $N_{HI} > 10^{20} cm^{-2}$. 21 cm emission studies also provide the signature of initial structure formation, star formation, radial velocities and mass of neutral hydrogen inside the galaxies. The first evidence of emission of 21 cm line was given by Ewen and Purcell (1951). Muller and Oort (1951) observed that gas has extended far more than the galaxy in optics region. Bera et al. (2019); CHIME Collaboration et al. (2022); Chowdhury et al. (2020); Wolz et al. (2022) are some of the examples of emission studies in which they try to evaluate the star formation rate and

neutral hydrogen distribution using GMRT radio telescope and in CHIME experiment to probe the large scale structure in the post-reionization era. Bharadwaj et al. (2001); Wyithe and Loeb (2009) use the power spectrum of the redshifted 21 cm intensity fluctuation to probe the statistical distribution of H I . Bharadwaj and Ali (2005); Bharadwaj et al. (2001) develop a methodology to estimate this H I power spectrum by using the radio interferometric observations from the unresolved H I clouds and that technique is known as Intensity mapping. They show that by correlating the directly observed quantity visibility by the interferometers in nearby baselines, it is possible to measure the H I power spectra unbiasedly. Following this work, several efforts are made to model the H I power spectra using analytic, semi-analytic models and simulations (Alonso et al., 2014; Bagla et al., 2010; Bharadwaj and Srikant, 2004; Wyithe and Loeb, 2009) including the H I bias (Castorina and Villaescusa-Navarro, 2017; Guha Sarkar et al., 2012; Mao et al., 2018; Sarkar and Bharadwaj, 2018; Sarkar et al., 2016) and the redshift space distortion effects (Hikage and Yamamoto, 2016; Jennings et al., 2012; Modi et al., 2019; Sarkar and Bharadwaj, 2019). These studies collectively provide a fair description of the expected redshifted 21 cm signal from the post-ionization era. The evolution of the 21 cm signal along different ages of the universe is shown in Fig 1.3.

Power spectrum of HI emission has also been used in the nearby universe to study the structure and dynamics of the interstellar medium of galaxies (Lazarian (1995), Dutta (2011)). In these studies, the intensity fluctuation in H I arises from both the column density and line of sight velocity fluctuations (Lazarian and Pogosyan, 2000). These studies show that the Interstellar medium is turbulent with a turbulence cascade ranging from a few kpc scales to a few pc scales. This energy cascade is found to regulate star formation and morphological evolution of the galaxies.

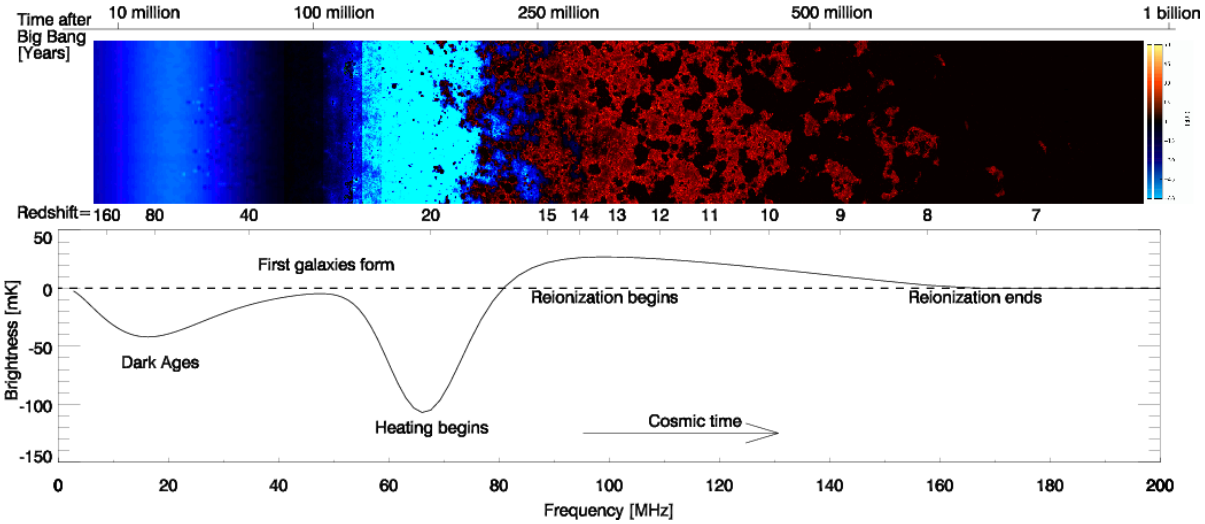

Figure 1.3: Shows the 21 cm evolution along various stages of the universe and is taken from (Pritchard and Loeb, 2012). The upper panel shows a slice through the light-cone of the 21 cm signal. The lower panel gives the evolution of the brightness temperature δT_b.

1.2 Gravitational Lensing

Gravitational lensing is the phenomenon of bending of light by gravity, which was first predicted by Einstein in 1915. The bending of light by gravity was first observed by Eddington during a solar eclipse in 1919 (Dyson et al., 1920). Einstein's original calculation was only for the sun-like stars, but later it was shown by Zwicky (1937) that larger objects in the universe, like galaxies (at that time they were called Nebulae) can bend the light and galaxy-galaxy lensing is also possible. Lensing by galaxies or other heavy masses was first observed with the discovery of twin quasars by Walshâ– et al. (1980) which was later confirmed as the two images of a single quasar by lensing phenomena. This phenomenon of lensing can be divided into three categories, first is strong gravitational lensing in which the galaxy clusters act as the lenses and the outcome is the formation of multiple images, the formation of the Einstein ring which is quite useful for observing the large distance objects (Bernstein et al., 1993; Wambsganss, 2001). The second is Weak lensing which we can't observe directly and requires large data to statistically measure, it is useful for the tomographic study of the universe (Hirata et al., 2007; Kaiser and Squires, 1993; Metzler

et al., 1999). Third is microlensing which is normally observed in the case of stars and is used to find the exoplanets (Bond et al., 2004; Udalski et al., 2005).

1.2.1 Lensing Basic

A brief discussion of lensing phenomena is given here. Fig 1.4 demonstrates the geometry of the gravitational lens system with D_d, D_{ds} and D_s as the angular diameter distance from lens to observer, lens to source and source to observer. The angular position of the source and image is $\vec{\beta}$ and $\vec{\theta}$ concerning the arbitrary optic axis. The magnitude of these distances is much larger as compared to the size of the source and lens. We can approximate the lens as a thin region from where this deflection occurs. This is known as a thin screen approximation. The mass distribution of the lens can then be projected along the line-of-sight and be replaced by a mass sheet orthogonal to the line-of-sight direction. The lens consists of various elements like dark matter halos and galaxies. The deflection angle $\vec{\alpha}$ at the position $\vec{\xi}$ can be approximated as

$$\vec{\alpha}(\vec{\xi}) = \frac{4G}{c^2} \int \frac{(\vec{\xi} - \vec{\xi}')\Sigma(\vec{\xi}')}{|\vec{\xi} - \vec{\xi}'|^2} d^2\xi'. \tag{1.7}$$

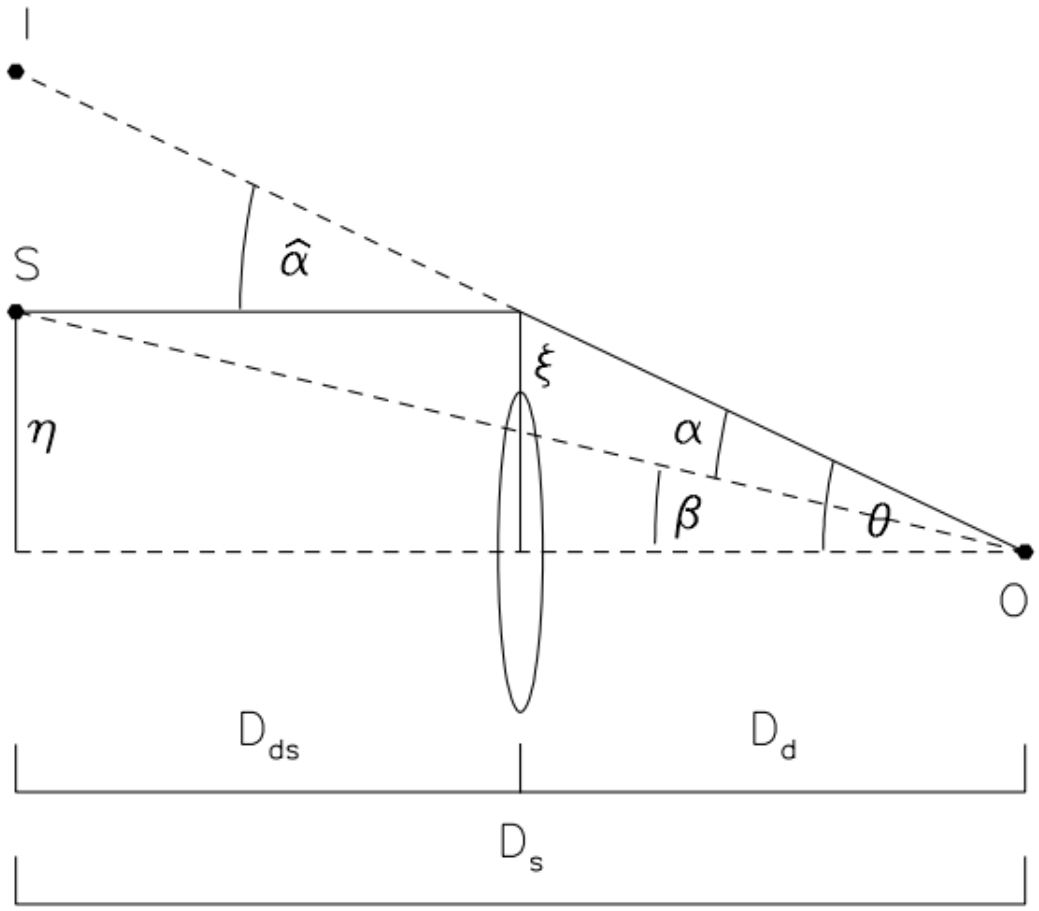

Figure 1.4: Lensing Geometry. The quantities D_d, D_{ds} and D_s represent the angular diameter distances between observer and lens (or deflector), lens and source, and observer and source. The angular position of the source (S) is defined as β, that of the image (I) is θ and the deflection angle is called α. ξ is the impact parameter of light ray. Figure is taken from Narayan and Bartelmann (1996)

This equation gives the deflection angle at the position $\vec{\xi}$ and $\vec{\xi}'$ represents the position of different elements in the lens. Σ represents the surface mass density at different positions in the lens. Position of image, source and deflection angle are related by the equation

$$\vec{\beta} = \vec{\theta} - \vec{\alpha}(\vec{\theta}). \tag{1.8}$$

This equation is known as the Lens equation or ray tracing equation. In the case of multiple imaging, this equation has multiple solutions of $\vec{\theta}$. Gravitational light deflection preserves surface brightness, but changes the apparent solid angle of a source. The total flux received from a gravitationally lensed image of a source is therefore changed in proportion to the ratio between the solid angles of the image and the source. We can write this deflection angle in terms of the scalar lens potential as

$$\psi(\vec{\theta}) = \frac{D_{ds}}{D_s D_d} \frac{2}{c^2} \int \phi(D_d \vec{\theta}, \mathrm{z}) d\mathrm{z} \tag{1.9}$$

here ϕ is the Newtonian gravitational potential of lens and ψ is the projected lens potential on the plane of sky, where z is the line of sight distance. The local properties of the lens mapping are described by a Jacobian matrix **A**

$$\mathbf{A} \equiv \frac{\partial \vec{\beta}}{\partial \vec{\theta}} = \left(\delta_{ij} - \frac{\partial \vec{\alpha}_i(\vec{\theta})}{\partial \vec{\theta}_j} \right) = \mathbf{M^{-1}} \tag{1.10}$$

where **M** is known the Magnification, under the geometric optics limit we can approximate it as the point spread function of the lens.

1.2.2 H I observation with gravitational lensing

We have previously seen that the 21 cm signal from neutral hydrogen can put light on the star formation, evolution and assembly of galaxies to form the galaxy clusters in the post-reionization era. But the 21 cm signal is very weak. Its amplitude is very small as compared to the galactic foreground signal (synchrotron emission) (Jelić et al., 2008; Trott, 2016). Pourtsidou and Metcalf (2015); Romeo et al. (2018) demonstrate the possible use of weak gravitational lensing for 21 cm intensity mapping using SKA-mid and SKA-low radio telescope to observe the lensed cosmological 21 cm signal at the redshift 2$\sim$3. This is further explored in Deane et al. (2015) for present and future radio telescopes. Jalilvand

et al. (2019) used the weak gravitational lensing to generate the intensity mapping power spectrum by perturbation theory. Metcalf and White (2009) put constraints on dark energy, dark matter and inflation using LOFAR and SKA by studying the gravitational lensing of high redshift 21 cm emission and then comparing with the constraints obtainable from wide-angle surveys of galaxy lensing. Saini et al. (2001) first investigated the idea of detection of neutral hydrogen from damped Lyman alpha cloud under certain restrictions on the column density in the H I cloud using the GMRT radio telescope at an observational frequency of 320 MHz. Blecher et al. (2019) report the first observation of lensed H I from a galaxy at redshift 0.4 using the GMRT. Lipnicky et al. (2018) observed eight spiral galaxies that are strongly lensing background sources where targets were selected from the Sloan WFC (Wide Field Camera) Edge-on Late-type Lens Survey (SWELLS) using the Arecibo, Karl G. Jansky Very Large Array, and Green Bank telescopes using signal to noise ratio of 6.7 and evaluate the mass of H I inside that galaxy of the order of 10^9 $M_\odot$. Dye et al. (2018) have detected strongly lensed highly star-forming galaxies using ALMA (henceforth ALMA*) observations.

There have been several approaches and studies to derive the lensing potential of galaxy clusters using optical observations (Cerny, 2018; Richard et al., 2010b, 2014; Sharon et al., 2020). Cerny (2018); Jauzac et al. (2015); Jullo et al. (2007); Richard et al. (2010b); Smith et al. (2005) use the different approaches to model the lensing potential using multiple images of the background galaxies. These lens models are then used to reconstruct the morphological properties of the galaxies at higher redshifts and infer their star formation and dynamical properties (Chirivì et al., 2020; Sharma et al., 2018). These studies have enriched our knowledge of the lensing potential over the last few decades.

*ALMA: Atacama Large Millimeter/Submillimeter Array, Chile (Wootten and Thompson, 2009)

1.3 Plan of the Thesis

The primary goal of this thesis is to explore the possibility of using the strong gravitational lensing by galaxy clusters to probe the neutral hydrogen in the post-reionization epoch of the universe. In this chapter, we discuss the background of our work. In Chapter 2, we discuss the matter power spectrum, 21 cm power spectrum and foreground power spectrum. In Chapter 3, we develop a formalism to calculate the power spectrum of the redshifted 21 cm signal using four simple gravitational lens models with strong gravitational lensing phenomena. In Chapter 4, we introduce an unbiased lensing based power spectrum estimator and calculate the uncertainties associated with this estimator. In the last Chapter, we summarise the thesis, make important concluding remarks, and point towards the future directions of this work.